Matrix Cracking in 3D Orthogonal Melt-Infiltrated SiC/SiC Composites with Various Z-Fiber Types

Gregory N. Morscher*
Ohio Aerospace Institute, Brookpark, OH

Hee Mann Yun*
Cleveland State University
Cleveland, OH

James A. DiCarlo
NASA Glenn Research Center
Cleveland, OH

ABSTRACT

The occurrence of matrix cracks in melt-infiltrated SiC/SiC composites with a 3D orthogonal architecture was determined at room temperature for specimens tested in tension oriented in the X-direction (parallel to Z-bundle weave direction) and Y-direction (perpendicular to Z-bundle weave direction). The fiber-types were Sylramic and Sylramic-iBN in the X and Y-directions and lower modulus ZMI, T300, and rayon in the Z-direction. Acoustic emission (AE) was used to monitor the matrix cracking activity. For y-direction composites, the AE data was used to determine the exact ($\pm$ 0.25 mm) location where matrix cracks occurred in the 3D orthogonal architecture. This enabled the determination of the stress-dependent matrix crack distributions for small but repeatable matrix rich "unidirectional" and the matrix poor "cross-ply" regions

---

* Senior Research Scientists residing at NASA Glenn Research Center, Cleveland, OH
Research supported by NASA's Ultra Efficient Engine Technology program

within the architecture. It was found that matrix cracking initiated at very low stresses (~ 40 MPa) in the "unidirectional" regions for the largest z-direction fiber tow composites. Decreasing the size of the z-fiber bundle, increased the stress for matrix cracking in the "unidirectional" regions. Matrix cracking in the "cross-ply" regions always occurred at higher stresses than in "unidirectional" regions, and the stress-dependent matrix crack distribution of the "cross-ply" regions was always over a wider stress-range than the "unidirectional" regions. For composites tested in the X-direction, a lower elastic modulus and a narrower and lower stress-range for matrix cracking were observed compared to composites tested in the Y-direction.

INTRODUCTION

The formation and propagation of multiple matrix cracks in relatively dense ceramic matrix composites when subjected to increasing tensile stress is necessary for high strength and tough composites [1]. However, the occurrence of matrix cracks at low stresses, especially for 2D architectures where 90^{o} tows act as matrix-flaws [2-3], may limit the structural capability of some non-oxide composite systems when subjected to oxidizing environments for long times at stresses sufficient to cause matrix cracking [4-6]. For 2D melt-infiltrated (MI) and chemical vapor infiltrated (CVI) SiC fiber-reinforced composites fabricated from the random lay-up of 0/90 fabric, the matrix cracking behavior in the 0^{o} direction has been well characterized for different fiber-types, constituent volume content, and tow ends per cm [7-8].

Three-dimensional (3D) orthogonal (Figure 1) architecture SiC/SiC composites are of interest because they offer potential benefits of better reproducibility, improved interlaminar mechanical properties [9-11] and, for the case of MI composites, potentially higher through-thickness thermal conductivity and better matrix infiltration [11]. It is important to understand how the 3D-orthogonal architecture affects matrix cracking in these composites. A thorough study on the accumulation of matrix cracks and the effect of matrix crack

accumulation on the stress-strain behavior was performed for a 3D-orthogonal composite with polymer impregnation and pyrolysis SiC matrix [9]. The amount and nature of stress-dependent matrix cracking was determined, was effectively modeled, and then was used to model stress-strain behavior. However, matrix-crack accumulation in three-dimensional (3D) architecture MI SiC/SiC composites with various fiber types in the Z-direction is not well understood.

Two aspects of 3D-orthogonal composites are of special interest. First, *how does the Z-direction tow fiber-type and size affect initiation and progression of stress-dependent matrix cracking in MI SiC/SiC composites when tested in the X or Y-direction?* Preliminary investigation of the mechanical behavior of MI composites with different z-direction fiber-type has been performed in reference 10. Second, *what effect does the local structure have on matrix cracking in the different regions of the orthogonal architecture (Figure 2)?* In the orthogonal architecture, especially when tested in the Y-direction (Figure 2b), there are small but repeatable regions that are essentially a matrix-rich unidirectional (UNI) composite with a z-direction tow perpendicular to the loading direction and another region that is a 0/90 cross-ply (XPLY) composite. With the improvement in acoustic emission (AE) technology [12,13], the determination of when, where, and how much matrix cracking occurs in these different regions can be accomplished.

Therefore, the focus of this study will be to answer these two questions for the 3D-orthogonal architecture melt-infiltrated (MI) composite system reinforced with SiC fibers studied in reference 11. In a companion paper [14], matrix cracking in 3D architecture composites will be compared to damage accumulation in 2D architecture composites.

EXPERIMENTAL

Unload-reload tensile tests were performed on melt-infiltrated SiC matrix composite panels that were fabricated using a 3D-orthogonal architecture with two different SiC fiber-types in the X and Y-direction and three different

fiber-types in the Z-direction. In general, all the composite architectures were reinforced in the X-Y fiber directions with 10 μm diameter Sylramic SiC fibers produced by Dow Corning and in the Z-direction by ZMI (Ube Industries), T300 (Amoco, US), and rayon (ICF Industries). After formation into flat X=230 mm by Y=150 mm preform panels with Z≈2 mm thickness, all the architectures (except for the 3D with rayon Z-fiber) were treated at NASA to convert the Sylramic fibers to the higher-performance Sylramic-iBN SiC fiber [15]. The Sylramic-iBN fibers in the preforms were then coated by chemical vapor infiltration (CVI) with BN interphase coatings and SiC matrices. Porosity between the CVI-coated "SiC/SiC mini-composite" tows was then filled by slurry infiltration of SiC particles, followed by molten infiltration of Si, commonly known as melt-infiltration, or MI* [16]. The composite panels were very dense, usually with less than 5% porosity, most of which was in the form of inter-tow porosity.

The 3D orthogonal panels (see Figure 1) were not balanced in-plane in terms of fiber content. In the X-direction, two Sylramic SiC fiber tows (800 fibers per tow) were combined and woven together at 3.95 tow-ends-per-cm (epcm), so that in the X-direction, single tows were effectively woven at 7.9 epcm at a fiber volume fraction of 15 to18%. For the Y-direction, single tows were woven at either 7.1 or 7.9 epcm for fiber fractions of 17 to 23%, respectively (see Table I). For the out-of-plane reinforcement, very low fiber volume fractions (<3%) were used based on the single-tow weaving of three different Z-direction fiber types: 11 μm ZMI SiC fibers from (800 fibers/tow); 7 μm T300 carbon fibers (1000 fibers/tow), and 12 μm polymer-derived rayon fibers from ICF Industries (400 fibers/tow). The X-Y fibers of the last architecture were not converted to Sylramic-iBN fibers because the rayon fiber is subject to decomposition at the elevated temperatures required for Sylramic-iBN treatment. As will be discussed, a key aspect of the Z-fiber types is their tow size in the final as-processed

---

* Interphase and matrix fabrication was performed by General Electric Power Systems Composites, Newark, DE

composite, which was largest for the ZMI fibers and smallest for the rayon fibers due to significant decomposition during composite fabrication. For convenience, the three different types of 3D orthogonal composites are referred to in this paper by their particular Z-fiber type. Table I summarizes all the key properties of the 3D architectures. Architectures and their composites will be referred to by the Z-direction fiber-type used.

Tensile tests were performed on specimens 12 mm wide by 150 mm long with a contoured gage section (dog-bone) of width 10 mm using a universal-testing machine (Instron Model 8562, Instron, Ltd, Canton Mass.) with an electromechanical actuator. Only the ZMI specimen was tested with the loading direction in the X-direction (Figure 2a) and the Y-direction (Figure 2b). All the other 3D composites were tested with the Y-direction oriented in the loading direction. Glass fiber reinforced epoxy tabs were mounted on both sides of the specimen in the grip regions and the specimens were gripped with rigidly mounted hydraulically actuated wedge grips. A clip on strain gage, with a range of 2.5% strain over 25.4 mm gage length was used to measure the deformation of the gage section.

Modal acoustic emission (AE) was monitored during the tensile tests with two wide-band, 50 kHz to 2.0 MHz, high fidelity sensors placed just outside the tapered region of the dog-bone specimen [13-14]. Vacuum grease was used as a couplant and mechanical clips were used to mount the sensors to the specimen. The AE waveforms were recorded and digitized using a 4-channel, Fracture Wave Detector (FWD) produced by Digital Wave Corporation (Englewood, CO). The load and strain were also recorded with the FWD. Location of the AE events was determined from the difference in times of arrival of the first peak, the measured stress-dependent speed of sound, and the distance between the two sensors as in references 11 and 12. However, the threshold technique typically used for determination of the time of arrival was not used. Instead, the time of arrival of the first peak of the extensional wave for each event waveform on the two sensors was determined by manual inspection

in order to get a location accuracy of less than +/- 0.25 mm*. In this way, the AE activity within the UNI and XPLY regions of the 3D composites oriented in the Y-direction (Figure 2b) could be distinguished.

Sections from the the gage section of the tested tensile specimens at least 10 mm in length were polished and then plasma (CF_4) etched at 500 W for 30 minutes. Etching was required to observe transverse matrix cracks; however, the etchant reacts with the free Si in the matrix, removing much of it, making it impossible to observe the extension of matrix cracks through the MI part of the matrix. Matrix cracks can only be observed in the dense CVI SiC layer between the BN and the MI matrix.

RESULTS

The stress-strain behavior for the different tensile specimens is shown in Figure 3 with key mechanical observations listed in Table II. The failure stress for all the composites was similar; however, not all the composites failed in the gage section. The elastic modulus of the ZMI composite oriented in the X-direction was significantly lower than that of the same composite oriented in the Y-direction (Table I). This is most likely due to the presence of the large "flat" Z-direction tow perpendicular to the loading axis for the X-direction orientation. There was also some difference in the debonding and sliding character in the BN interphase region. The ZMI composite exhibited debonding and sliding in between the Sylramic-iBN fiber and the BN interphase (inside debonding) as is typical for most MI composites. However, the other two Z-direction fiber-type composites exhibited a mixture of inside debonding and outside debonding, that

---

* The accuracy was dependent on the resolution in the time-domain, the separation distance of the sensors, and the speed of sound across the material. For this study, those parameters were 0.1 microseconds, 50 mm, and ~ 9000 m/sec for a pristine composite, respectively. As matrix cracking occurs, the speed of sound decreases, which was measured during the test from AE that occurred outside the sensors [12], i.e., in the grips or tapered section of the dog-bone, resulting in more accurate event location.

is, debonding and sliding between the fibers and BN interphase and between the BN interphases and the CVI SiC matrix, respectively. Outside debonding and mixed inside and oustide debonding composites have been shown to have lower interfacial shear strengths for MI composites than purely inside debonding composites[17].

Y-DIRECTION ORIENTED COMPOSITES

The location of AE activity versus applied stress is plotted in Figure 4 for the ZMI composite Y-direction. The data is separated into the highest decade of energy (high energy), the second highest decade of energy (mid energy), and the lowest three decades of energy (low energy). The crack density for these systems with this modal AE approach has been shown to be nearly directly proportional to AE energy [12-13]. Also shown in Figure 4 is a schematic of the 3D orthogonal architecture commensurate with the location of the tested specimen. It is clear that initial AE activity occurs in the UNI regions of the 3D orthogonal composite at stresses below 50 MPa. This is significantly lower than typical 2D MI composites where first AE activity occurs at ~ 100 $\pm$ 20 MPa [7,18]. Initial AE activity was composed of lower energy events, probably tunnel cracks [8,19] that emanated from the Z-bundle. At ~ 115 MPa, high-energy events occurred in the UNI region, signifying large matrix crack formation and growth. Significant AE activity did not occur in the XPLY region until stresses greater than 140 MPa.

The AE activity in the UNI and XPLY regions is plotted as cumulative AE energy for each 1.5 mm length section in Figure 5. Significant cumulative AE activity in the UNI region increases very rapidly starting at ~ 115 MPa with increasing stress over a narrow stress-range. AE activity diminishes above ~ 175-200 MPa in the UNI region which would correspond to near matrix crack saturation in the UNI region. However, for the XPLY regions, significant cumulative AE activity begins to occur at a slightly higher stress (130 MPa) to the UNI regions, but the distribution of cumulative AE energy is over a very wide

stress range and does not appear to cease even up to failure, i.e., the XPLY region does not appear to saturate with matrix cracks up to the fracture stress of the specimen. It is also apparent that AE energy in the UNI region was significantly higher in magnitude than the XPLY region. Evidently, matrix cracks in the denser, higher modulus matrix-region are of a higher energy than those formed in the predominantly 90° bundles of the XPLY region. Figure 6 shows a region of the double-ZMI specimen tested in the Y-direction orientation and the matrix cracks which occur in the UNI region. The matrix crack density in the UNI regions for this specimen averaged ~ 10.2 cracks/mm. Similarly, the matrix crack density in the XPLY region for this specimen averaged ~ 8.8 cracks/mm (Table II).

Figure 7a shows the AE data from Figure 5 for the two different regions, i.e., UNI and XPLY. All the data for the UNI and XPLY regions of the specimen were combined and normalized by the cumulative AE energy at failure for the ZMI composite. The same approach was taken for the T300 and rayon composites tested in the Y-direction and are plotted in Figure 7a as well. The normalized cumulative AE energy was then multiplied by the final crack density (Table II) to determine an estimated stress-dependent matrix crack density [7] for the different regions of each specimen (Figure 7b). The matrix cracking stress-ranges are higher for T300 and rayon composites in both the UNI and XPLY regions with rayon composites having the highest matrix cracking stress-range for both regions.

For the UNI region, most of the matrix cracking for a given specimen occurs over a narrow stress range with the mid stress of the distribution increasing with decreasing Z-direction tow size. The height of the Z-direction tow is ~ 0.15 mm for ZMI, 0.11 mm for T300, and 0.03 mm for rayon when measured from polished longitudinal sections as in Figure 5 where the z-direction tow is closest to the face of the composite. When measured in the interior of the composite, the tow-height increases to 0.40, 0.28 and 0.15 mm for ZMI, T300 and rayon, respectively. Figure 8 shows the small rayon tow height. Note that

the rayon fiber was expected to have decomposed during the CVI BN step; however, some porous carbon char remained in the form of what appears to be an approximately 60 "fiber" tow (Figure 8).

For the XPLY region, significant matrix cracking always occurs at much higher stresses than the UNI region for the same composite. The stress-ranges for matrix cracking are nearly identical for T300 and rayon composites. The ZMI composite matrix crack stress-range is somewhat broader in the XPLY region; however, it encompasses the stress-range of the other two composites. In addition, the ZMI composite has a lower load-bearing fiber volume fraction. It will be shown in the companion paper [14] that matrix cracking in the XPLY region is for the most part dependent on the volume fraction of the composite constituents and the cross-ply structure.

Fibers in the rayon composite were very straight in both the UNI and XPLY regions compared to the other z-tow composites, e.g., ZMI (Figure 6). This may also contribute to the high matrix crack stresses for this composite. It was quite remarkable that the very first cracks (as detected by AE) in the rayon composite occurred at ~ 170 MPa, significantly higher (at least 40 MPa) than the other two composites or any other 2D MI composite tested to date.

X-DIRECTION ORIENTED COMPOSITE

Only the ZMI composite was tested in the X-direction orientation (Figure 3). The UNI length scale (~ 0.3 mm) for the X-direction was too small to discern AE events in that region. Figure 9 shows the total cumulative AE energy versus applied stress for both the X-direction oriented and Y-direction oriented (UNI and XPLY data combined) ZMI specimens. Low energy AE activity occurs at relatively low stresses similar to that for the ZMI composites tested in the Y-direction, presumably due to tunnel crack formation in the large Z-fiber tows. Significant AE activity for the X-direction oriented composite started at the same stress as the Y-direction orientation; however, the stress range for matrix cracking of the X-direction orientation was significantly narrower than the Y-direction composite.

DISCUSSION

In this study, two factors of 3D orthogonal composites were found that clearly dictate the nature of matrix cracking: (1) the size or height of the z-fiber tow and (2) the local architecture of the composite (at least when tested in the Y-direction). It will be shown in the companion paper [14] that the lower stress and narrow stress-range for matrix cracking when tested in the X-direction is due to the larger size (number of fibers) of the load-bearing Sylramic fiber tows oriented in the X-direction (compared to composites tested in the Y-direction with standard size tows). However, the low stresses at which tunnel crack formation occurred for the X-direction oriented ZMI composite was presumably due to the large Z-direction tow in the 3D architecture.

For the Y-direction test, a larger Z-fiber tow height will generally result in lower matrix cracking stresses, i.e., the Z-fiber tow is the largest flaw in the "matrix". Note that in Figures 4 and 5, for the ZMI composites tested in the Y-direction, a significant amount of low energy AE events occur between ~40 and 115 MPa. This corresponds to tunnel cracking in the Z-fiber tow. For the ZMI composites, high AE energy events begin to occur at 115 MPa in the UNI region and a high rate of cumulative AE energy continues with increasing stress corresponding to large fiber-bridged matrix crack growth and/or formation which leads to through thickness cracking. For the T300 and Rayon composites, there was no lower stress range where only low AE energy events occurred in the UNI region. Instead, high-energy events and a high rate of cumulative AE energy occurred at the onset of AE activity (Figure 7), i.e., ~ 130 MPa and ~ 170 MPa for T300 and Rayon composites, respectively. This implies that the stress required to cause a matrix crack to propagate through thickness of the UNI region [1] in the ZMI composite is about 115 MPa. However, for the higher fiber volume fraction (Y-direction) T300 and Rayon composites, no flaws existed that would form matrix cracks below 130 and 170 MPa, respectively.

The implication for elevated temperature exposure in oxidizing environments is obvious: lower stress-rupture capability for larger Z-fiber tow sizes. If a large Z-fiber tow size is necessary for improved interlaminar properties, then use-stress in the X or Y-direction may have to be sacrificed. However, if one is attempting to improve thermal conductivity, matrix infiltration, or achieve straighter load-bearing fibers then smaller Z-fiber tows may be sufficient.

The difference in matrix cracking stress-range for the UNI and XPLY regions of Y-direction oriented composites is striking. It will be shown in the companion paper [14] that the stress-range for matrix cracking in the rayon XPLY region exceeds that attained in 2D composites. One implication of the significant differences in matrix cracking stresses for the different local architectures is the potential for designing components with different local architectures for the desired properties most needed in that location. For example, it may be possible to engineer a woven structure for a component that offers high interlaminar stresses in one area, high matrix cracking strength in another, and high thermal conductivity in another.

CONCLUSIONS

Matrix cracking in 3D-orthogonal, melt-infiltrated SiC/SiC matrix composites was studied for composites with different z-direction fiber-types. The stress-range where matrix cracking occurred was dependent on the z-direction tow size and the local architecture. The smaller the z-direction tow size (height), the higher the composite stress-range where matrix cracking occurred. It was also found that in the region of the structure that was essentially "cross-ply", matrix cracks formed at higher stresses than in adjacent matrix-rich "unidirectional" regions. These findings must be considered when 3D-orthogonal structures are desired for elevated temperature applications where the use of the 3D architecture to achieve the desired through-thickness property could lead to strength-degradation in tension due to oxidation of the interior of the composite

through low-stress forming matrix cracks. However, understanding the effect of architecture on matrix cracking stress could be used advantageously to engineer desired structures where areas of a component require high through-thickness properties and other areas of the same component require high tensile matrix crack strengths.

REFERENCES

1. J. Aveston, G.A. Cooper, and A. Kelly, "Single and Multiple Fracture: The Properties of Fiber Composites," pp. 15-24 in The Properties of Fibre Composites, Conference Proceedings, National Physical Laboratory (Guildford, U.K.). IPC Science and Technology Press, Ltd., Teddington, U.K., 1971
2. J-M. Domergue, F.E. Heredia, and A.G. Evans, "Hysteresis Loops and the Inelastic Deformation of 0/90 Ceramic Matrix Composites," *J. Am. Ceram. Soc.*, **79** [1] 161-70 (1996)
3. P. Pluvinage, A. Parvizi-Majdi, and T.W. Chou, "Damage Characterization of Two-Dimensional and Three-Dimensional Braided SiC-SiC Composites," *J. Mater. Sci.*, **31** 232-241 (1996)
4. F.E. Heredia, J.C. McNulty, F.W. Zok, and A.G. Evans, "Oxidation Embrittlement Probe for Ceramic-Matrix Composites," *J. Am. Ceram. Soc.*, **78** [8] 2097-100 (1995)
5. G.N. Morscher, J. Hurst, and D. Brewer, "Intermediate-Temperature Stress Rupture of a Woven Hi-Nicalon, BN-Interphase, SiC-Matrix Composite in Air," *J. Am. Ceram. Soc.*, **83** [6] 1441-49 (2000)
6. G.N. Morscher and J.D. Cawley, "Intermediate Temperature Strength Degradation in SiC/SiC Composites," *J. European Ceram. Soc.*, **22** 2777-2787 (2002)
7. G.N. Morscher, "Stress-Dependent Matrix Cracking in 2D Woven SiC-fiber Reinforced Melt-Infiltrated SiC Matrix Composites," submitted to *Comp. Sci. Tech*

8. G.N. Morscher, "Matrix Cracking in Four Different 2D SiC/SiC Composite Systems," to be published in 35th International SAMPE Technical Conference Proceedings, Dayton, OH (2003)
9. T. Ogasawara, T. Ishikawa, H. Ito, N. Watanabe, and I.J. Davies, "Multiple Cracking and Tensile Behavior for an Orthogonal 3-D Woven Si-Ti-C-O Fiber/Si-Ti-C-O Matrix Composite," *J. Am. Ceram. Soc.*, **84** [7] 1565-74 (2001).
10. G. Ojard, T. Araki, S. Nishide, K. Watanabe, G. Linsey, J. Anderson, "Material Characterization of 3-D Orthogonal Reinforced Ceramic Matrix Composites," *Ceram. Eng. Sci. Proc.*, **23** [3] 599-606 (2002)
11. H.M. Yun, J.Z. Gyekenyesi, and J.A. DiCarlo, "Effects of 3D-Fiber Architecture on Tensile Stress-Strain Behavior of SiC/SiC Composites," Ceram. Eng. Sci. Proc., 23 [3] 503-510 (2002)
12. G.N. Morscher, "Modal Acoustic Emission of Damage Accumulation in a Woven SiC/SiC Composite," *Comp. Sci. Tech.* **59** 687-697 (1999)
13. G.N. Morscher, "Modal Acoustic Emission Source Determination in Silicon Carbide Matrix Composites," in Review of Progress in Quantitative Nondestructive Evaluation, eds. D.O. Thompson and D.E. Chimenti, CP 509, American Institute of Physics, pp. 383-390 (2000)
14. G.N. Morscher, "Comparison of Matrix Cracking in 3D Orthogonal and 2D Woven SiC/SiC MI Composites" J. Am. Ceram. Soc., submitted
15. H.M. Yun and J.A. DiCarlo, "Comparison of the Tensile, Creep, and Rupture Strength Properties of Stoichiometric SiC Fibers," *Cer. Eng. Sci. Proc.*, **20** [3] 259-272 (1999)
16. D. Brewer, "HSR/EPM Combustor Materials Development Program" *Mater. Sci. Eng. A*, **A261**, 284-291 (1999).
17. G.N. Morscher, H.M. Yun, J.A. DiCarlo, and L. Thomas-Ogbuji, "Effect of a BN Interphase that Debonds Between the Interphase and the Matrix in SiC/SiC Composites," *J. Am. Ceram. Soc.*, in print

18. G.N. Morscher, J.Z. Gyekenesi , and R.T. Bhatt, "Damage Accumulation in 2-D Woven SiC/SiC Ceramic Matrix Composites," in Mechanical, Thermal and Environmental Testing and Performance of Ceramic Composites and Components, ASTM STP 1392, M.G. Jenkins, E. Lara-Curzio, and S.T. Gonczy, Eds., pp. 306-319 (2000)
19. B.N. Cox and D.B. Marshall, "Crack Initiation in Fiber-Reinforced Brittle Laminates," *J. Am. Ceram. Soc.*, **79** [5] 1181-88 (1996)

Table I: Properties for three types of 3D Architectures

Z-direction Fiber-type	X and Y direction Fiber-type	Y tow ends per cm (epcm)[f]	Y fiber fraction	X fiber fraction	Z fiber fraction
ZMI[a]	Syl-iBN[d]	7.1	0.174	0.152	0.032
T300[b]	Syl-iBN	7.9	0.226	0.178	0.014
Rayon[c]	Sylramic[e]	7.9	0.203	0.160	0.001

[a] Ube Industries, 800 fibers per tow, average fiber diameter ~ 11 μm
[b] Amoco, 1000 fibers per tow, average fiber diameter ~ 7 μm
[c] ICF Industries, 400 fibers per tow, average fiber diameter ~ 12 μm
[d] NASA modified Sylramic fiber – by heat treatment of the Sylramic fiber to produce a thin, ~ 100 nm, in-situ BN layer on the surface of the fiber
[e] Dow Corning, Midland MI; 800 fibers per tow, average diameter ~ 10 μm
[f] for all three architectures, 3.95 epcm of a double tow was woven in the X-direction

Table II: 3D Composite Mechanical Properties*

Composite Z-direction Fiber-type	E, GPa	t, mm	Interphase Debonding	Failure Location	Failure Stress, MPa	Crack Density: UNI/XPLY(avg) # per mm
ZMI (Y direction)	248	2.05	Inside	Gage	317	10.2 / 8.8 (9.2)
T300 (Y direction)	237	1.75	Mixed	Gage	345	7.4 / 4.3 (5.9)
Rayon (Y direction)	238	1.95	Mixed	Radius	336	4.8 / 4.0 (4.4)
ZMI (X direction)	205	1.92	Inside	Radius	322	12 / 7.2 (7.9)

* At lest two specimens from each panel were tested for each composite architecture with all the specimens performing very similar to one another. However, the data shown is only for the one specimen that the detailed AE analysis was performed on.

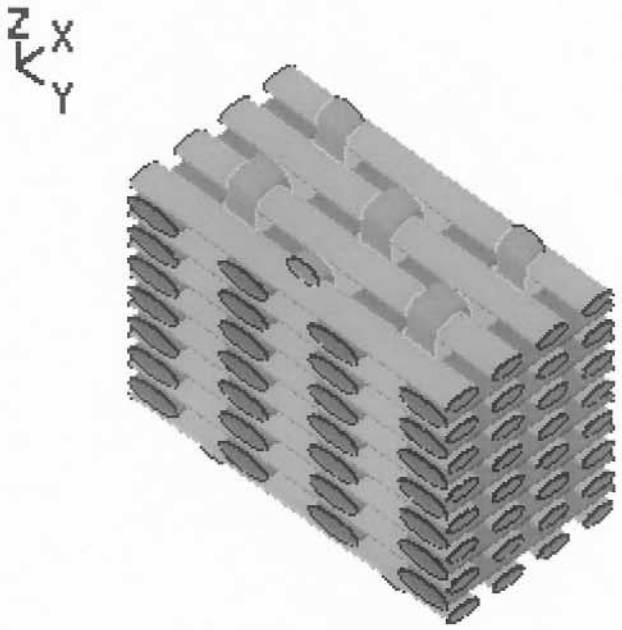

Figure 1: Schematic representations of 3D orthogonal architectures. Each architecture contained 8 layers of Y-direction single-tow fiber and 7 layers of double-tow fiber.

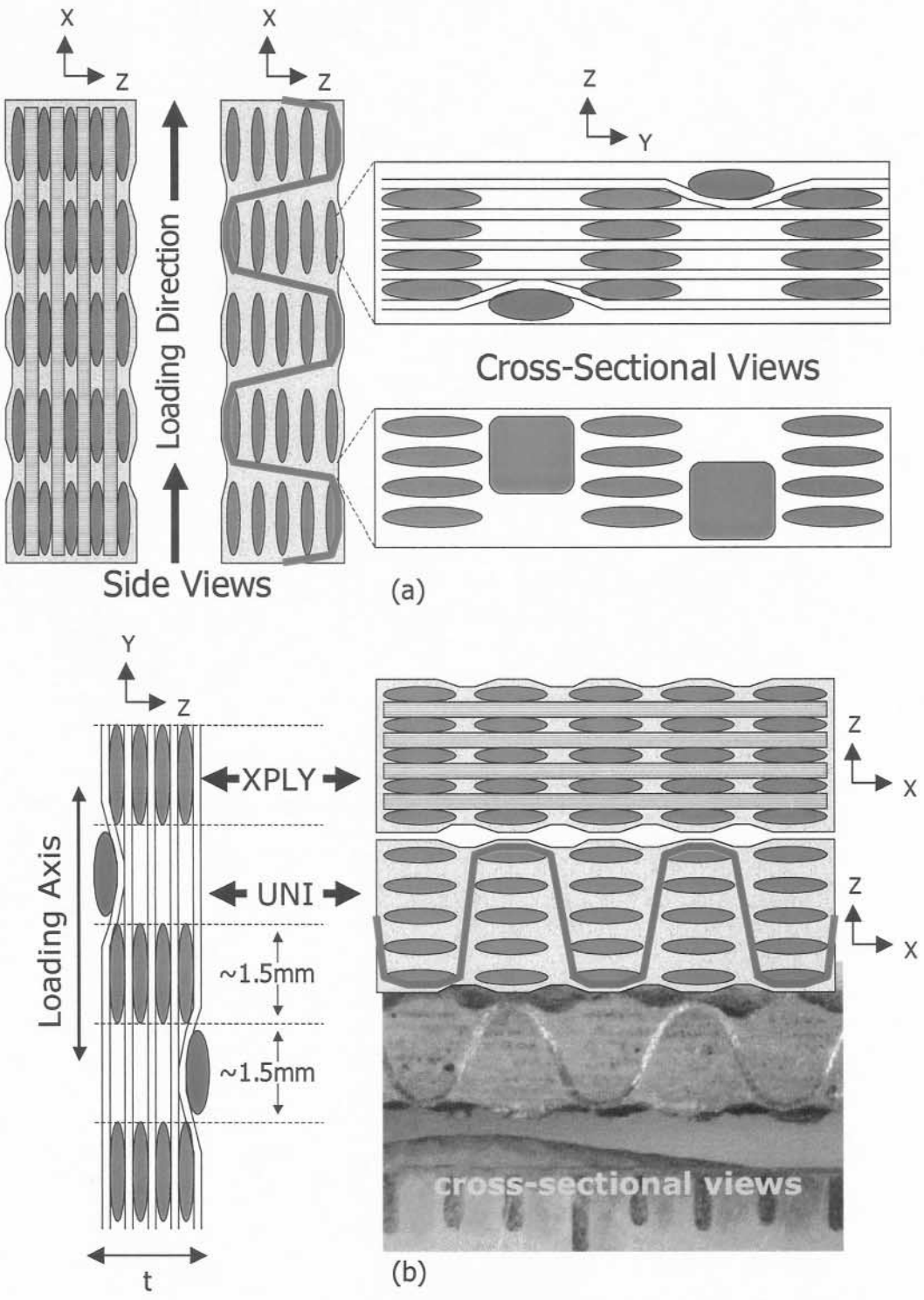

Figure 2: Schematic representation of 3D orthogonal composite aligned in the (a) X-direction and (b) Y-direction. Only nine layers are represented in these schematics, the composites actually contained fifteen layers (see Figure 1).

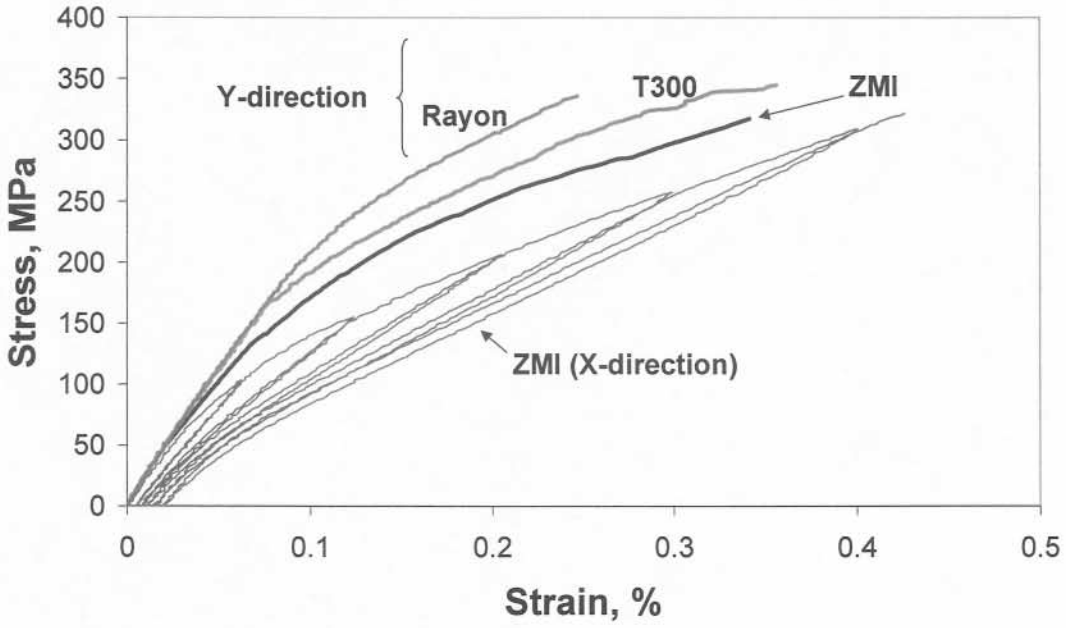

Figure 3: Stress-strain data for composites tested in the X and Y-direction. The hysteresis loops were removed from the Y-direction composite data for clarity.

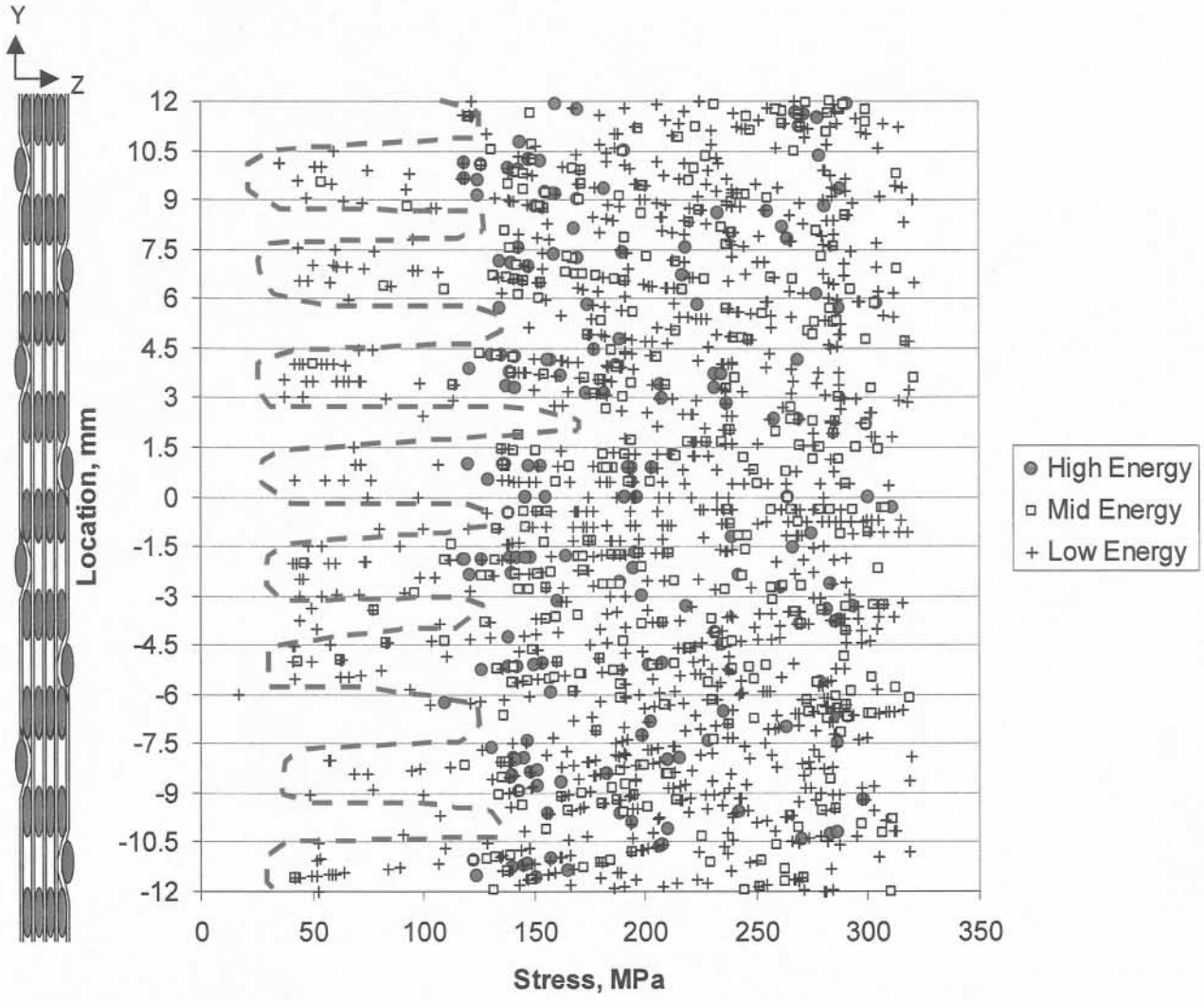

Figure 4: Location of AE events along the length of a ZMI specimen oriented in the Y-direction.

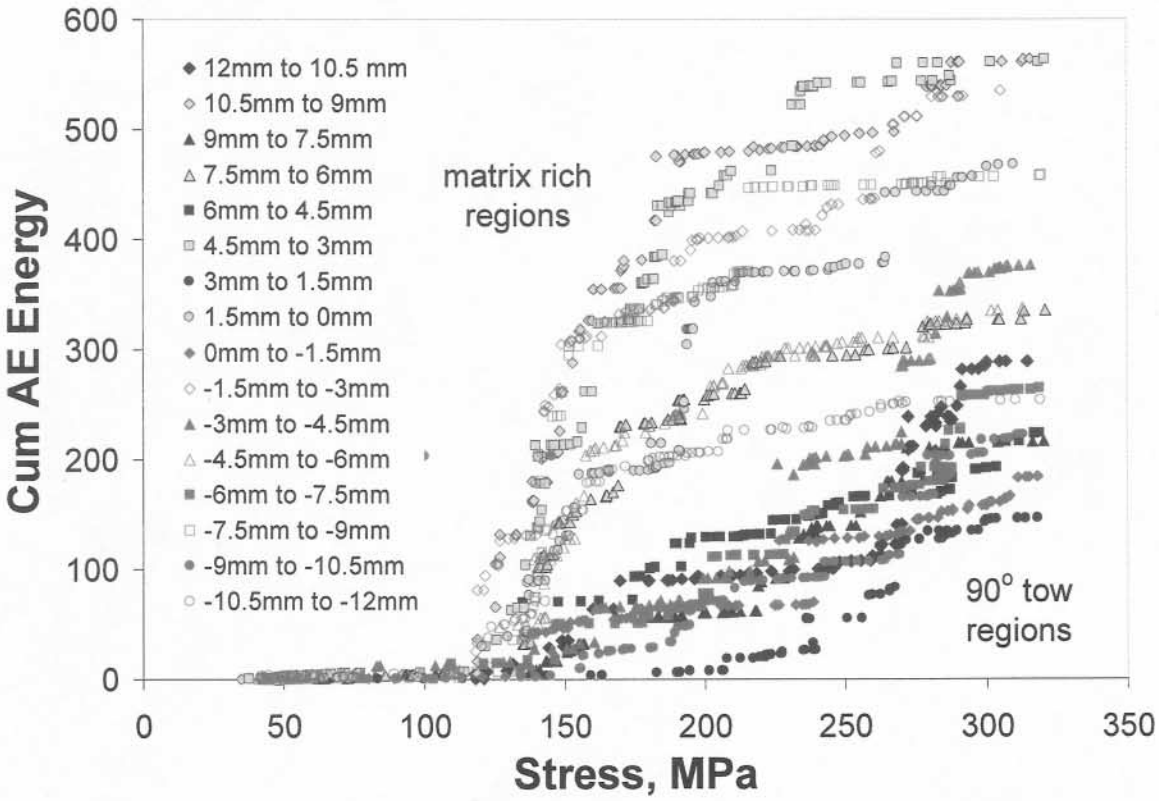

Figure 5: Cumulative AE energy for each 1.5 mm region corresponding to the UNI or matrix rich regions and the XPLY or 90° tow regions.

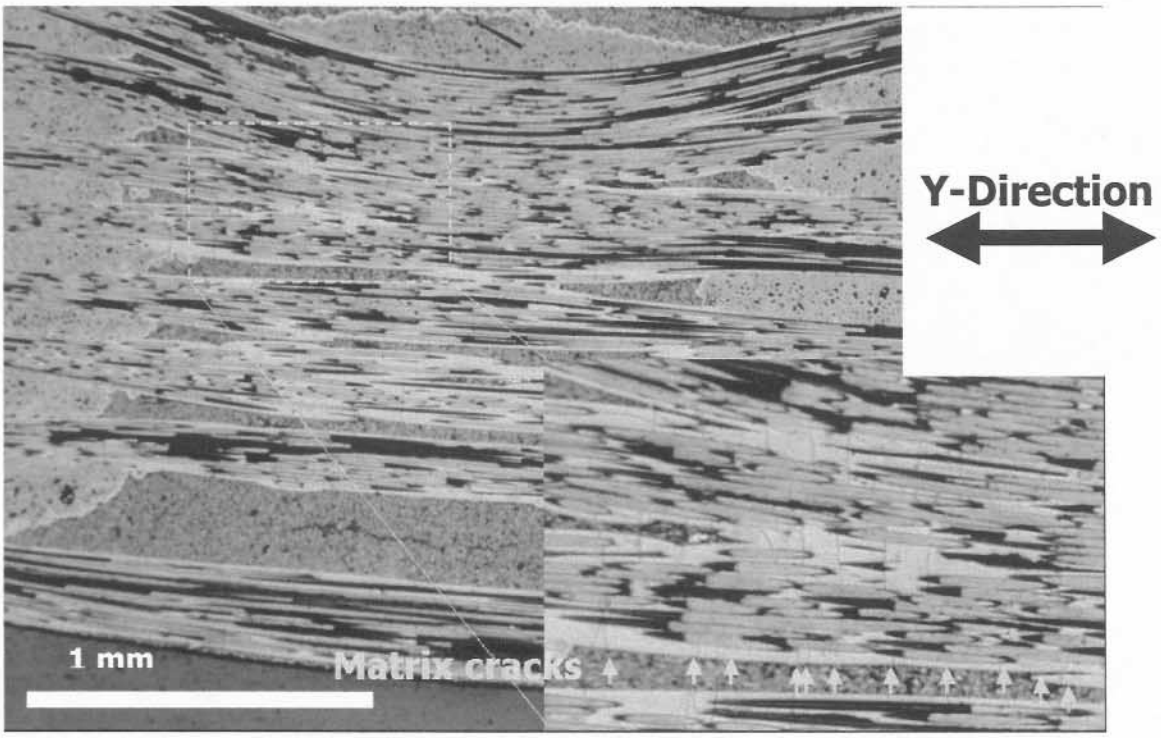

Figure 6: Polished longitudinal section of double ZMI specimen tested in the Y-direction orientation.

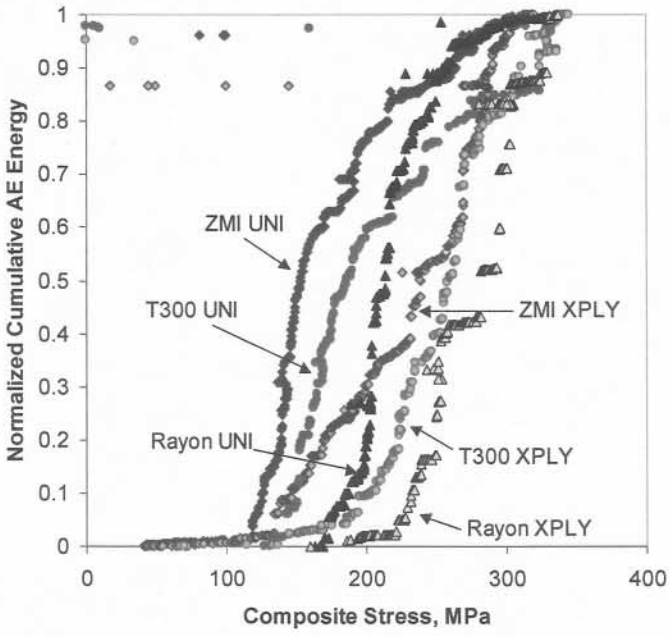

(a)

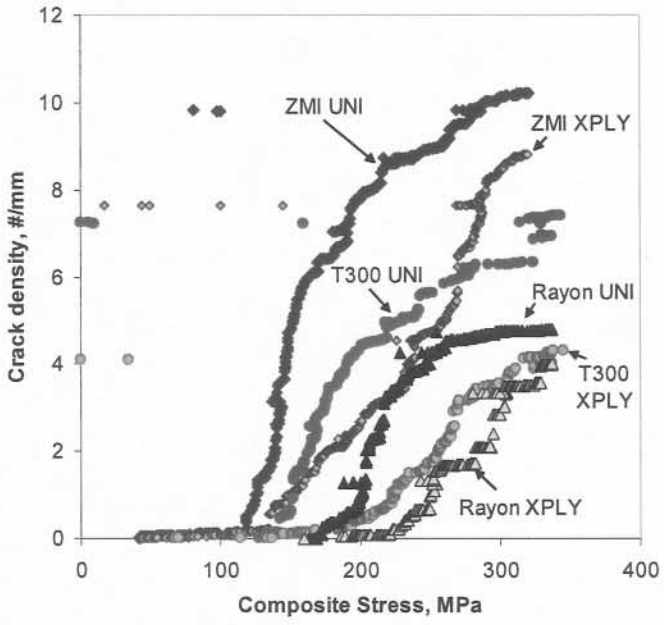

(b)

Figure 7: Comparison of the normalized cumulative AE energy versus composite stress for the UNI and XPLY regions of the three different z-fiber tow composites tested in the Y-direction orientation.

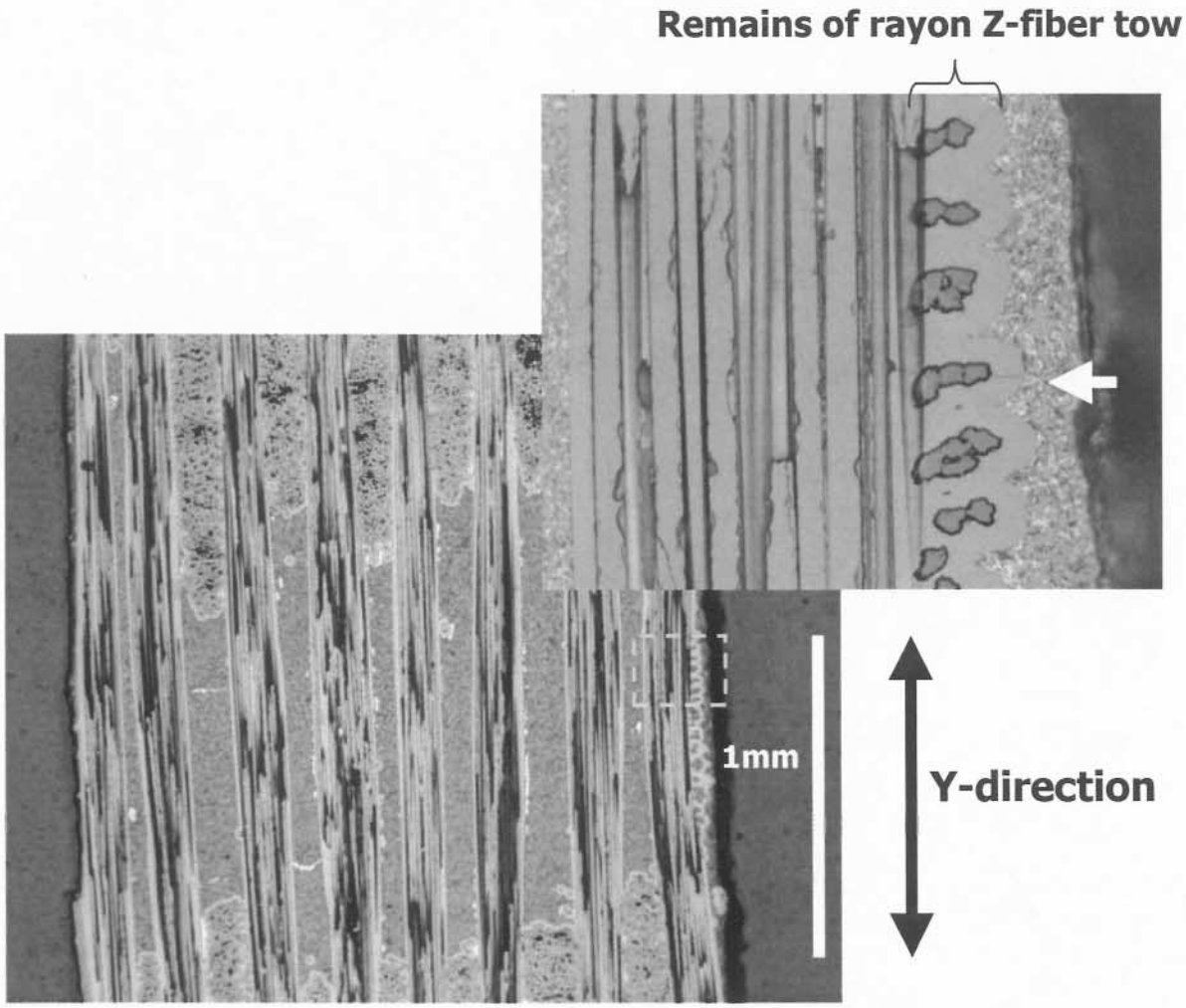

Figure 8: Polished longitudinal section of Rayon specimen tested in the Y-direction orientation. Arrow indicates a matrix crack.

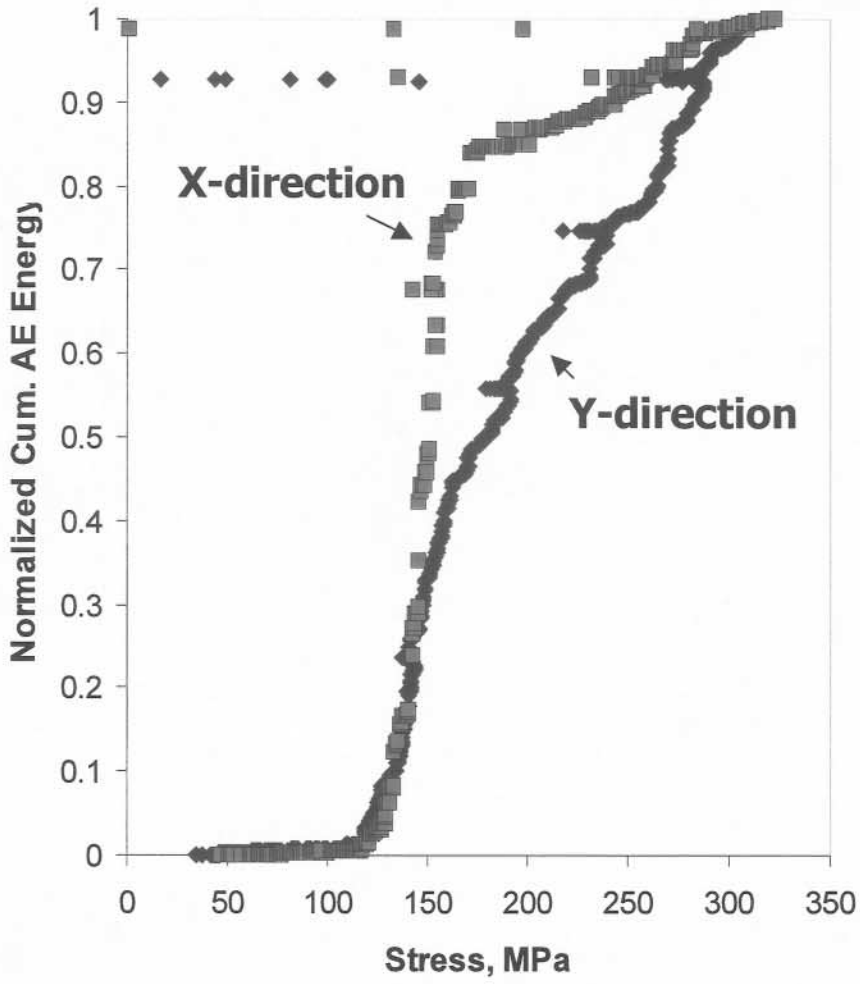

Figure 9: Normalized cumulative AE energy for double ZMI composites tested in the X-direction and the Y-direction.